——ONLINE FIRST(NOT Peer-Reviewed)——

Title：Oil Spill Detection Using Otical Sensors: A Multi-Temporal Approach

Author：Roberto Luciani 1

Institute/Affiliation：1 Sapienza University of Rome

Received：2018-09-07

Accepted：2018-09-20

Process：1、First trial(Field and check) ✓

2、Peer review ☐

3、Editing and three trials ☐

4、Published online ☐

Company Registration No.: 201427293E
7030 Ang Mo Kio Avenue 5#04-155
Northstar @ AMK Singapore (569880)
www.Whioce.com

Oil Spill Detection Using Otical Sensors: A Multi-Temporal Approach

LUCIANI Roberto[1*], LANEVE Giovanni[1]
[1] School of Aerospace Engineer (SIA), Sapienza University of Rome, Rome, Italy
*Corresponding Author: Roberto Luciani, Via Salaria 851, 00138, Italy;
roberto.luciani@uniroma1.it

Abstract: Oil pollution is one of the most destructive consequences due to human activities in the marine environment. Oil wastes come from many sources and take decades to be disposed of. Satellite based remote sensing systems can be implemented into a surveillance and monitoring network. In this study, a multi-temporal approach to the oil spill detection problem is investigated. Change Detection (CD) analysis was applied to MODIS/Terra and Aqua and OLI/Landsat 8 images of several reported oil spill events, characterized by different geographic location, sea conditions, source and extension of the spill. Toward the development of an automatic detection algorithm, a Change Vector Analysis (CVA) technique was implemented to carry out the comparison between the current image of the area of interest and a dataset of reference image, statistically analyzed to reduce the sea spectral variability between different dates. The proposed approach highlights the optical sensors' capabilities in detecting oil spills at sea. The effectiveness of different sensors' resolution towards the detection of spills of different size, and the relevance of the sensors' revisiting time to track and monitor the evolution of the event is also investigated.

Keywords: Oil spill; MODIS; Landsat 8; change vector analysis; Gulf of Mexico; Refugio; Zakynthos

1. Introduction

The accurate detection of oil spill at sea from optical and radar images, primarily consists in the reduction of look-alikes and false positives. Remote sensing of oil slicks at sea takes advantage of the image contrast variation between oil and surrounding waters. In radar imagery the contrast variation is the result of the dampening of the water surface roughness only eventually caused by oil. Surfactant agents (mainly biogenic in nature), water currents runoff, rain cells, freshwater slicks and wind patterns can eventually result in oil spill look-alikes [1—2].

Remote sensing satellite platforms have widely demonstrated their capabilities in detecting oil spills at sea using visible, infrared, and radar-based techniques [3—5].

Although Synthetic Aperture Radar (SAR) systems are, nowadays, the first choice in the field of oil spill detection, there are several pitfalls to be accounted for. SAR systems can provide all-weather day and night acquisition at high resolution over the area of interest. On the other hand, SAR performs poorly in discriminating look-alikes and can be completely ineffective outside the optimal wind speed range. The SAR systems operational capabilities

are also limited by the low revisiting frequency and, in some cases, the high cost of the data [6].

Satellite based optical sensors can be successfully employed in detecting and describing oil spills. In optical data, oil spills are either characterized by a negative contrast (dark patches over the image) or a positive contrast (bright patches over the image) [7—9]: contrast variations depends on the observation angle with respect to the relative position of the sun. When the angle describing the sensor observation direction, deviates from the condition of specular reflection with respect to the sun (sun glint), the higher scattering of the rough sea surface surrounding the oil, determines the negative contrast. In case of sun glint condition, the oil-dampened surface is the one to appear brighter [9]. The contrast intensity depends not just by the angles of illumination and observation, but also by the oil optical properties, oil thickness, sea water light absorption and scattering coefficients, state of the sea surface (depending mostly by the wind patterns), sea depth and sea bottom conformation [10].

Ma *et al.* [11] and Lammoglia *et al.* [12] defined the spectral signature of oil spills, basing their studies on laboratory experiences and theoretical models, with the aim to isolate the regions of the electromagnetic spectrum more sensitive to oil spill. Oil in general shows higher reflectance than seawater; in coastal zone, however, seawater may show higher reflectance than oil because of sediments and suspended materials from land. Zhao *et al.* [13] provides a wide range of oil spectral characteristic from several Arabian Gulf oil spill cases, both for sun glint and sun glint-free conditions and in presence of numerous look-alikes. According to [13—14], oil spills in sun glint conditions can also be detected as anomalies in the sea surface texture; or else, outside sun glint conditions, detecting techniques can rely only on oil spectral characteristics.

Hu *et al.* and Zhao *et al.* [13—15], largely demonstrated the possibility of successfully employing MODIS data to detect oils spills in estuary and coastal areas, through several images per week and despite the limitations imposed by the weather conditions. Bulgarelli *et al.* [16—17], explored the inter–relationship between reflectance and absorption of an oil spill to unpolluted sea water, proving the capabilities of MODIS also in oil spill detection applications. The presence of sun glint contamination is the most favorable condition in which an oil spill can be detected, because the mirror effect of oil on water greatly aids the specular reflection. The oil spill detection in MODIS glint-contaminated imagery was investigated by [18].

OLI/Landsat 8 optical data are available since 2013; OLI data using VIS/NIR channels with high spatial resolution (30 m) and thermal channels (100 m) have been largely employed in oil spill detection task and its efficiency has been sufficiently investigated. Oil spill were detected in coastal bay using OLI VIS/NIR channels by [19—20]. Oil film differs from sea water in thermal characteristics and absorption of sun rays energy. Thermal infrared channels were employed by [21] in detecting the Gulf of Mexico oil spill.

The mono-temporal approach could be ineffective in detecting oil spills: the oil spill features might not be easily detected due to 1) the low quality of the image, 2) complexity of the oil spill scenario and 3) possible multiple targets (false positive and look-alikes). Oil spill detection and discrimination tasks can be effectively and efficiently solved by multi-temporal approaches through a Change Detection (CD) framework [22]. Change Vector Analysis (CVA)

is a CD technique and a robust approach for detecting and characterizing radiometric change in multispectral remote sensing datasets. Radiometric changes are highlighted and characterized through the analysis of change within the images multispectral/multitemporal domain [23]. The CVA technique has been effectively applied to both MODIS and OLI datasets. Land-Cover change detection using multi-temporal MODIS NDVI data was carried out by [24]. The possibility of using 250 m MODIS metrics (from 16 days composites) in change vector analysis (CVA) to map wetland dynamics in the Linyanti wetland (Namibia) between 2001 and 2010 was investigated by [25]. Change vector analysis and Fuzzy c-means classification (FCM) algorithm were applied to derive shoreline positions as the transition zone between the classes water and non-water in shorelines mapping and monitoring applications using OLI data by [26]. A perspective to solve the oil spill detection problem using Landsat 8 and HJ-1 (Huan Jing-1: Environmental Protection & Disaster Monitoring Constellation) imagery through CVA analysis is investigated by [27]. In particular, a coarse-to-fine multitemporal change analysis procedure is designed to investigate the spectral–temporal variation of change targets located in the scenario.

This study investigates the application of change vector analysis to MODIS and OLI Landsat 8 top of atmosphere optical imagery in detecting oil spill at sea. The goal is to demonstrate the effectiveness of change detection as a systematic and automatic approach in detecting and discriminating oil spills in both multitemporal and multispectral domain. The developed methodology is independent from the solar-view geometry and atmospheric conditions.

We accomplished the detection of oil spill from MODIS and Landsat OLI data using VIS/NIR channels. For each pixel, we computed the CVA intensity and the CVA direction, within the observation period. Both the change vector intensities and the corresponding change directions are necessary to interpret the changes occurring at sea and discriminate oil spill from look-alikes. MODIS and OLI sensors are characterized by different operational capabilities. We highlight 1) the MODIS Terra and Aqua satellites high revisiting frequency against 2) the Landsat OLI high resolution. We demonstrated 3) the MODIS capabilities of tracking and monitoring an oil spill event over a period and 4) the Landsat OLI capabilities of detecting small oil spills and even natural outflows. Three study areas have been selected to test the proposed methodology; each one of them is characterized by a well-documented oil spill event. The oil spills differ from source, oil quality and thickness, extension and oil-in water emulsion.

2. Data and Study Area

2.1 Study Area

Three study areas have been used in this investigation. The first area (Figure 1, a) is the Gulf of Mexico (US), where the Deepwater Horizon crisis took place in 2010. The oil leak was detected on the afternoon of April 22, 2010, when a large oil slick began to spread at the former rig site. It flowed for 87 days. It is considered to be the largest marine oil spill in the history of petroleum industry with an estimated total discharge of 4.9 million barrels [28].

The second area (Figure 1, b) is located immediately north of Refugio State Beach in Santa Barbara County, California (US). In May 2015, a corroded pipeline, named Line 901,

deposited 3,400 barrels of crude oil into the sea.

The third area (Figure 1, c) is located off the coast (6 km heading south) of Zakynthos island (Greece). This area has been pointed out by [29—30] to be the location of a natural oil outflow, providing natural oil spills during summer every year.

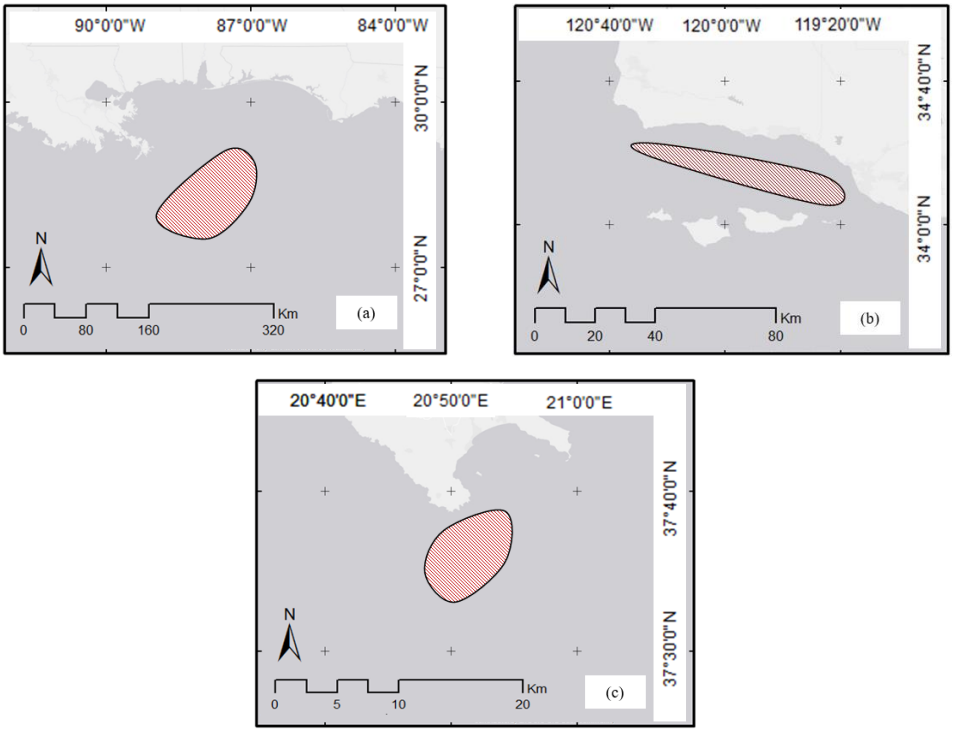

Figure 1. Study areas: (a) Gulf of Mexico (US); (b) Refugio State Beach, Santa Barbara County (US); (c) Zakynthos Island (GR).

2.2 Study Area

MODIS and OLI Landsat 8 data have been used in this work. MODIS images, bands 1 (620-670 nm), 2 (841-876 nm), at 250 m spatial resolution, were selected to investigate the oil spill in the Gulf of Mexico. The Refugio and Zakynthos oil spills were investigated using OLI Landsat 8 images, bands 1(433-453 nm) and 2 (450-515 nm), 4 (636–673 nm), 5 (851–879 nm), at 30 m spatial resolution. The list of images used to investigate the oil spills is shown in Table I; the list of reference images, used to carry out the change detection analysis, is shown in Table II.

The images were preprocessed and converted from DN (Digital Numbers) to reflectance TOA (Top Of Atmosphere) values. The refractive index of oil is greater than the one of sea water, but there is the possibility of masking the data while performing atmospheric correction, as demonstrated by [31]. Therefore, the images were not atmospherically corrected.

Study area	Date	Sensor	Glint	Name
G.M. (US)	25 Apr 2010	MODIS	on	MYD02QKM.A2010115.1855.061.2018059233544
G.M. (US)	27 Apr 2010	MODIS	off	MOD02QKM.A2010117.1705.061.2017254171904
G.M. (US)	27 Apr 2010	MODIS	off	MYD02QKM.A2010117.1840.061.2018060013742

G.M. (US)	29 Apr 2010	MODIS	on	MOD02QKM.A2010119.1655.061.2017255001900
G.M. (US)	09 May 2010	MODIS	on	MYD02QKM.A2010129.1905.061.2018059224710
G.M. (US)	17 May 2010	MODIS	on	MOD02QKM.A2010137.1640.061.2017251223855
G.M. (US)	25 May 2010	MODIS	on	MYD02QKM.A2010145.1905.061.2018060053906
G.M. (US)	27 May 2010	MODIS	on	MYD02QKM.A2010147.1855.061.2018060085407
G.M. (US)	04 Jul 2010	MODIS	on	MOD02QKM.A2010185.1640.061.2017251225037
R. (US)	30 Aug 2015	OLI	off	LC08_L1TP_042036_20150830_20170225_01_T1
Z. (GR)	06 Aug 2017	OLI	off	LC08_L1TP_184034_20170806_20170813_01_T1
Z. (GR)	29 Aug 2017	OLI	off	LC08_L1TP_185034_20170829_20170914_01_T1

G.M.= Gulf of Mexico; R.=Refugio; Z.=Zakynthos

Table 1. Datasets

Study area	Date	Sensor	Name
G.M. (US)	25 Apr 2010	MODIS	MOD02QKM.A2006263.1635.061.2017196025514
G.M. (US)	27 Apr 2010	MODIS	MOD02QKM.A2009081.0145.006.2014230210254
G.M. (US)	30 May 2009	MODIS	MOD02QKM.A2009150.1640.061.2017299013020
R. (US)	11 Oct 2013	OLI	LC08_L1TP_042036_20131011_20170308_01_T1
R. (US)	14 Dec 2013	OLI	LC08_L1TP_042036_20131214_20170307_01_T1
R. (US)	15 Jan 2014	OLI	LC08_L1TP_042036_20140115_20170307_01_T1
Z. (GR)	02 Feb 2016	OLI	LC08_L1TP_183034_20160202_20170330_01_T1
Z. (GR)	24 Jan 2016	OLI	LC08_L1TP_184034_20160124_20170330_01_T1
Z. (GR)	09 Jul 2016	OLI	LC08_L1TP_185034_20160709_20170323_01_T1

G.M.= Gulf of Mexico; R.=Refugio; Z.=Zakynthos

Table 2. Reference Images

3. Methodology

The proposed methodology is presented below in three separate sections. First, the general image processing and data preparation is presented for both MODIS and OLI data. Then Change Vector Analysis principles are recalled and the very foundation of CVA based features extraction explained. Finally, the CVA is applied to the oil spill detection task; a training site is analyzed to highlights the CVA capabilities in discriminating oil spill at sea.

3.1 Image preprocessing

Clouds removal and land masking automatic procedures were developed. Errors induced by the presence of clouds over the area of interest can be significantly reduced through clouds removal. MODIS bands 1, 2, 26 and 31 were selected to be employed into a set of binary tests to detect clear sky conditions over the area of interest following the procedure described in [32-34]. Landsat 8's BQA (Band Quality Assessment) image was used as described in [35], to remove clouds from OLI data. Cloud contaminated pixels were not restored and were considered lost to the oil spill detection following procedure. Sun glint conditions, both over MODIS and OLI, data were detected using the Cox & Munk isotropic sun glint model [36]. Land masks for MODIS and OLI images, were developed using the NDWI (Normalized Difference Water Index) according to [37]. The CD analysis effectiveness is related to the

quality of the images taken as base reference. In order to reduce the errors induced by reference images variability, a selection of oil free and cloud free images of the study areas was acquired and processed over a period of roughly one year. For each study area three reference images have been selected: a new reference image was built out of the average of the original three.

3.2 Change Vector Analysis (CVA)

Change Vector Analysis (CVA) is a multi-temporal and multi-spectral change detection technique. Using a change vector, resulting from images comparison over a multi-temporal archive, the CVA can characterize changes in the multi-spectral space. CVA is a multi-variate technique, which accepts the desired number of bands from the input pairs. The multi-dimensional space, in which the CVA operates, is comprised between these bands. Multi-spectral remote sensed data are then represented as coordinates of such a vector in the multi-dimensional space defined by the selected spectral components. The change vector is described by its length (magnitude of the change between the data pairs), and its direction (angle of the change) [38]. Once applied to the multi-temporal analysis task, the CVA compares the differences in the time-trajectory of biophysical variables or indicators [39]. Let I_H be the reference image acquired at time t_1 (oil and cloud free), and I_G the current image, acquired at time t_2 over the same scenario to investigate a suspected oil spill. The multi-dimensional space is defined by the number of bands (n) in the image. For a given pixel, the change vector in the n-dimensional space is defined as shown in Equation 1.

$$ED = G - H \quad \text{where} \tag{1}$$
$$G = (g_1, g_2, \Lambda\ , g_n)^T$$
$$H = (h_1, h_2, \Lambda\ , h_n)^T$$

Where H and G are the image pixel vectors, respectively at time t_1 and t_2, containing n bands.The change magnitude ($\|ED\|$) is computed as the Euclidean Distance (ED) between vector end-points (Euation. 2) [23].

$$\|ED\| = \sqrt{(g_1 - h_1)^2 + (g_2 - h_2)^2 + \Lambda\ + (g_n - h_n)^2} = \sqrt{X_1^2 + X_2^2 + \Lambda\ + X_n^2} \tag{2}$$

The change angles are defined as the ratio between the spectral differences and the change magnitude (Equation 3).

$$\cos\ \theta_i = \frac{X_i}{\|ED\|} \quad (i = 1, \mathrm{K}\ , n) \tag{3}$$

An example of a change pixel in a bi-dimensional space is depicted in Fig. 2. Thresholds should be determined to discriminate pixels that change from no-change pixels. On the other hand, the direction of the change vector facilitates the discrimination among different types of change that can possibly occur.

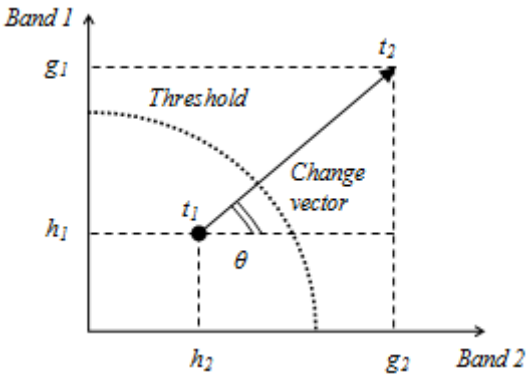

Figure 2. Change vector in two bands radiometric space

3.3 Oil spill detection

Oil spill detection is carried out by the CVA as a binary recognition task in the bi-temporal and multi-spectral domain. The ultimate objective is to isolate anomalies from sea background and discriminate oil spills among the possible look-alikes.

We selected two different sensors to investigate oil spill events that differs by oil type, spill overall extension and oil thickness. MODIS data, at 250m spatial resolution, has been selected to investigate the potential of high revisiting frequency (1-2 days) multispectral imagery in oil spill monitoring applications. Despite the low revisiting frequency (16 days), we investigated the effectiveness of OLI data in detecting oil spills of moderate extension and thickness (ca. 2,000 barrels).

According to [18,40] uncorrected features at 469, 555 and 649 nm are capable to show significant indications of oil. At the same time optical imagery in the near-infrared (859 nm) proved to be effective in oil spill detection. MODIS band 1 (620-670 nm) and band 2 (841-876 nm) have been selected for the oil detection task over the Gulf of Mexico. The corresponding OLI bands have also been selected to attempt the same detection task, using the same technique, over the other two study areas (Refugio beach and Zakynthos). OLI sensor is called to investigate two peculiar oil spill events: a leakage and a natural outflow both characterized by high degree of oil emulsion with water and reduced spill thickness.

The OLI higher resolution with respect to MODIS, is necessary to investigate oil spill of small dimension but the nature of the spill it should be also taken into account. Switching from one sensor to the other just to improve the spatial resolution is not enough to perform the detection the task. In these particular case, the OLI bands 1 (433-453 nm) and 2 (450-515 nm) have also been called in to take advantage of the reflectance of oil at those wavelengths despite the presence of the atmospheric effect [40—41]. The overall procedure workflow is presented in Figure 3. Once the image preprocessing is completed, the CVA takes place. The analysis is carried out on a pixel base, between each data pair constituted by the current image under analysis and the reference image of the area of interest. As result, a change vector is released for each pixel. Then, the magnitude and direction of the change vector are retrieved and submitted for a binary test. Using the reported oil spill from May 17, 2010 as training site, both numerical and angular thresholds have been extracted and employed within the final testing of the previously extracted change vector characteristics. A change pixel is recognized when the magnitude exceeds the numerical threshold, while the nature of the change is

pointed out by the angular direction. If the change direction is comprised within the angular range retrieved for oil spill from the training sites, then the pixel is marked as contaminated.

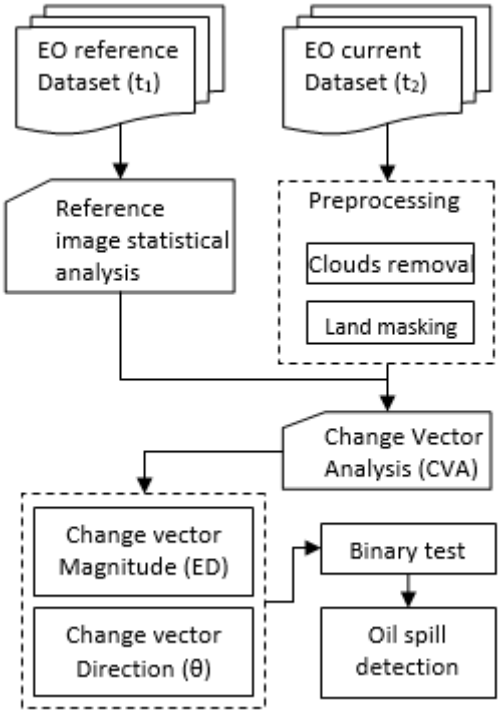

Figure 3. Oils spill detection procedure overall workflow

The MODIS Terra (16:40 UTC) image undergone the CVA analysis, then several transects of the oil spill were selected to be analyzed. Figure 4 highlights two transects (A and B) of the reported spill, used to empirically assess the numerical thresholds of the detection algorithm. Those transects have been selected to comprise a different number of oil-water transitions. Transect A is characterized by six oil-water transitions (h, i, l, m, n, o) across the spill main body, while transect B is characterized just by two transitions (p, q) across the spill tail, which is likely to be the spill's thinnest section.

Change vector's magnitude and direction for both the transect A and B are reported respectively in Figure 5 and 6. Each oil-water transition is well marked by the magnitude change for both transects. Several minimum values between 0.1-0.3 and maximum values between 0.4-0.6 were tested to assess a set of discriminating thresholds: if exceeding the threshold minimum value, the pixel is undergoing a change. The nature of the detected change is compatible with the presence of oil at sea only if 1) the pixel's magnitude does not exceed the threshold maximum value and 2) the change direction is compatible with oil spill features. The settled thresholds have been used in detecting oil spills with both MODIS and Landsat 8 images. However, the oil spill quality (in terms of spill thickness and oil-water emulsion level) reported for Refugio Beach and Zakynthos Island, led us to review (and in particular to lower) the detecting thresholds. Oil spill features are related with change vector directions that fall within the angular range comprised between 40 °- 50 °degrees.

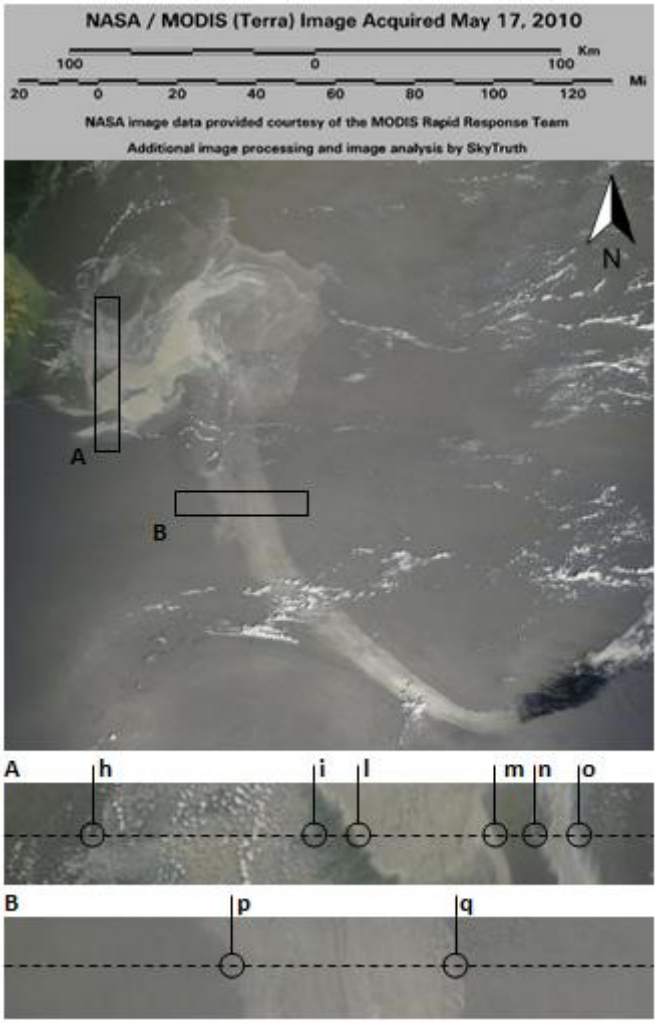

Figure 4. Transect A-B over the training site; transects details in which the sample line and the oil-water transitions are highlighted.

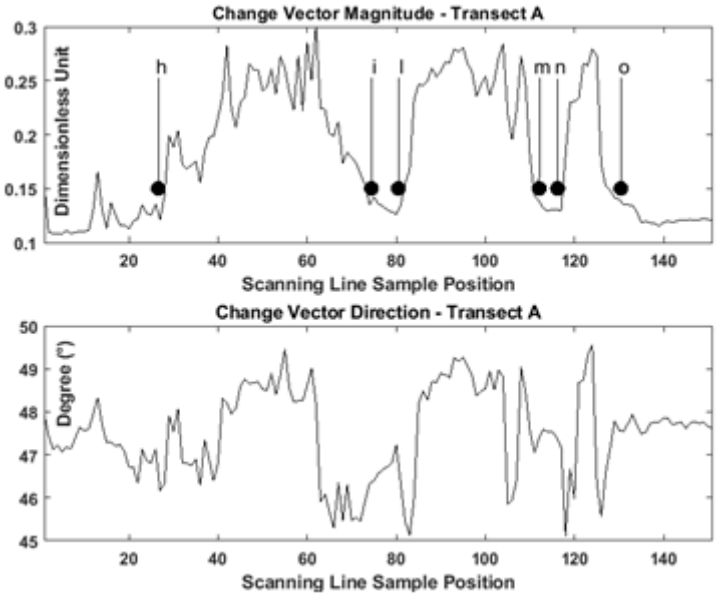

Figure 5. Change vector's magnitude and direction for transect A with the reported oil-water transitions.

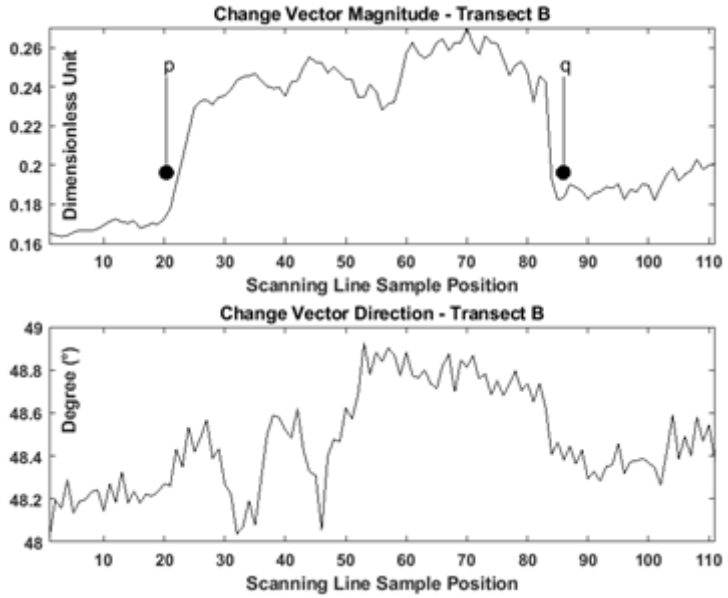

Figure 6. Change vector's magnitude and direction for transect B with the reported oil-water transitions.

4. Results

To identify the numerical response of oil-water transitions to the CVA analysis, change vector profiles along transect A and B were plotted. The visual interpretation of the oil-water transitions allows to identify a significant signature of oil in the multi-temporal/multi-spectral domain. On these bases, two combinations of change vector's magnitude and direction values were identified to carry out the oil spill detection. Oil spill discrimination was carried out using a pixel-based binary test with the aim to (1) identify if the pixel had undergone a change in the multi-temporal domain (testing the change vector magnitude); and (2) to ascertain if the eventually detected change is related or not to oil spill contamination (testing the change vector direction). As it is already mentioned, the shorter wavelengths are more sensitive to oil, therefore OLI Landsat 8 data in bands 1 and 2 were preferred to bands 3 and 4 to investigate oil spill of limited extension and/or natural outflow.

Figure 7a-n, presents the classification results for the proposed methodology over the selected study areas. The Gulf of Mexico oil spill is a well documented case study: field samples were collected during May 7, 2010 by Clark *et al.* [42] and the oil spill patches detected in Figure 7a-h are in accordance with accurate image interpretation carried out by the Skytruth team on MODIS and RADARSAT images [43]. No ground truth was available for the remaining areas: the Refugio beach oil spill detection is in accordance with Skytruth reports [44], while the Zakynthos natural outflow is a well known area largely investigated by [29—30].

All the images from the Gulf of Mexico were under sun glint contamination excepting the ones from April 27, 2010 (Figure 7, b-c). The images taken from Refugio beach and Zakynthos are glint free. The oil spill detection was carried out independently from the sun

glint contamination of the area of interest. Then, in the context of the proposed methodology, sun glint conditions have not been recognized as a privileged condition of observation.

The change vectors associated with the oil spill reports are provided by means of polar scatter plot in Figure 7 (a_1-n_1). Each plot represents the change vector's end position of the cloud free pixels at sea over the area of interest. Table III provides a complete overview of these results. The MODIS data analysis was carried out using Bands 1 and 2 at 250m spatial resolution in both glint free and glint contaminated conditions. The threshold of the change vector magnitude is comprised between 0.15-0.5. Threshold values are only slightly risen by glint contamination; therefore the previous identification of glint contaminated pixels can be used to switch the magnitude threshold towards the proper minimum value to carry out the detection task.

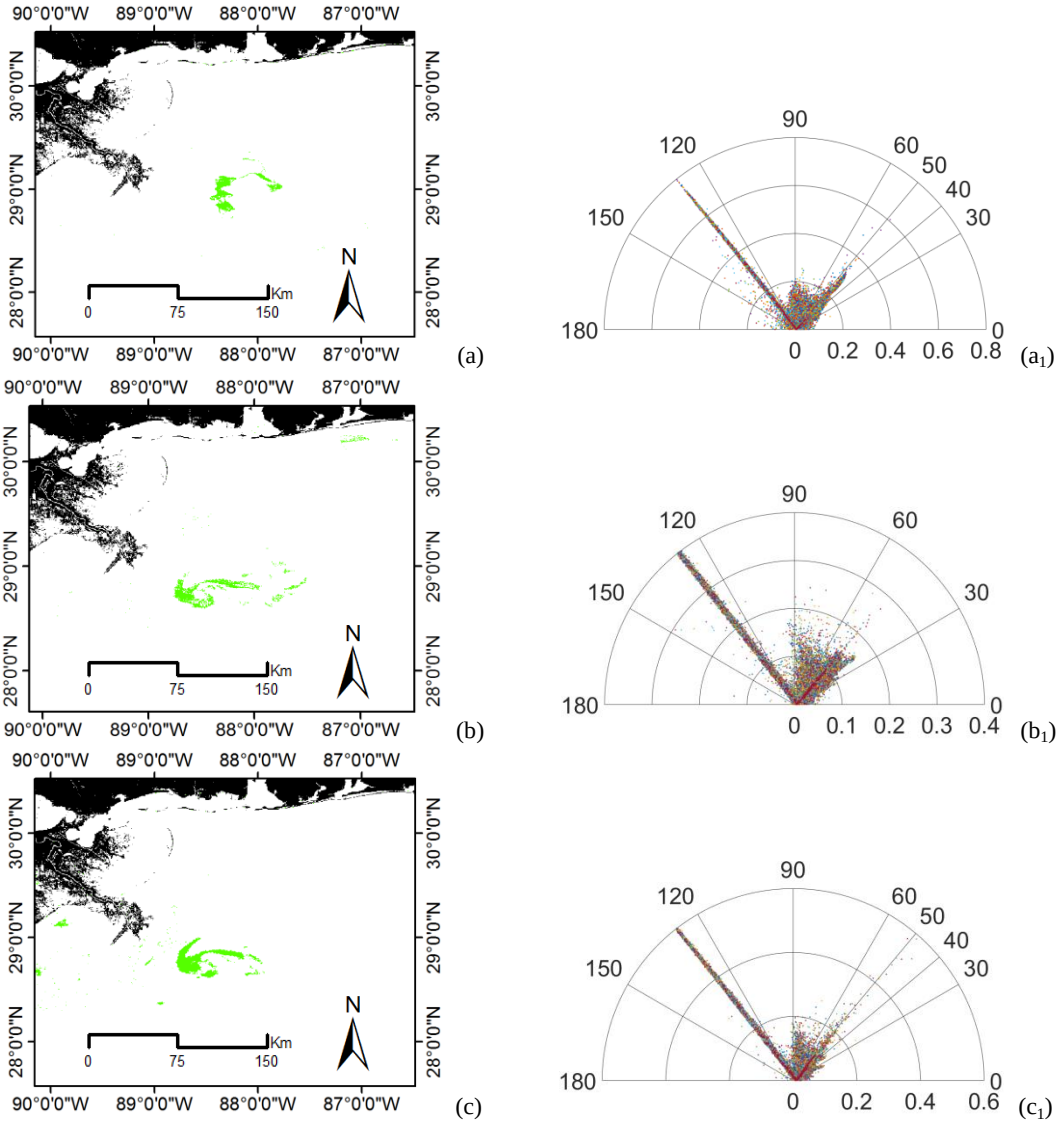

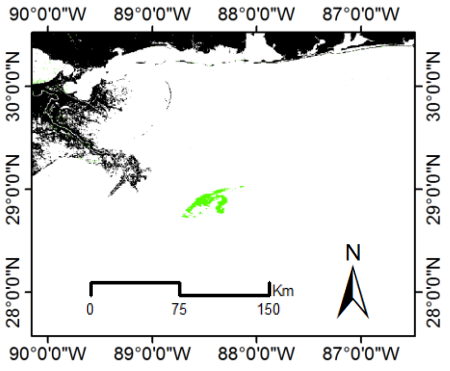

(d)

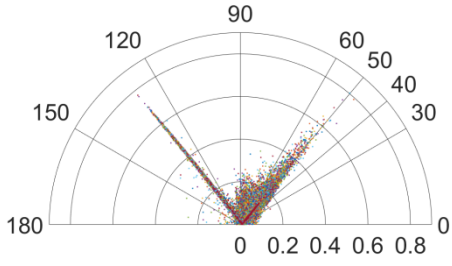

(d_1)

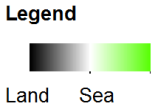

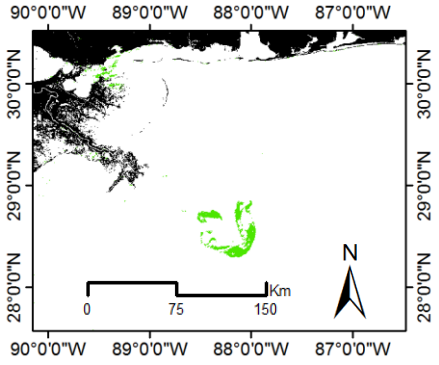

(e)

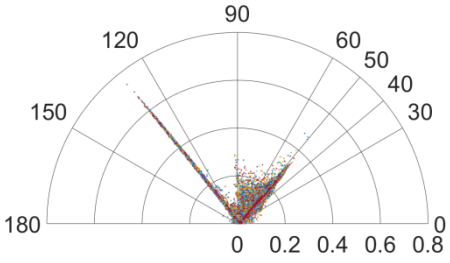

(e_1)

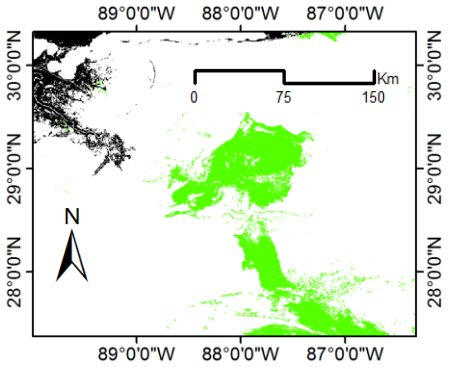

(f)

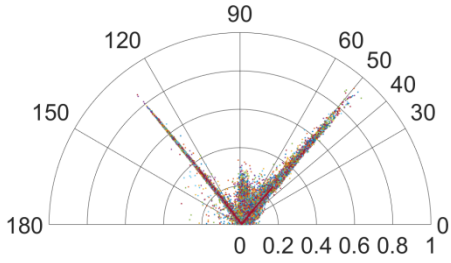

(f_1)

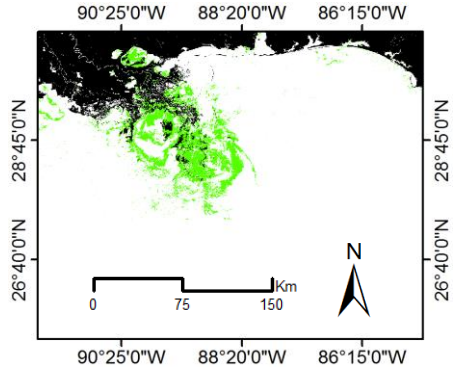

(g)

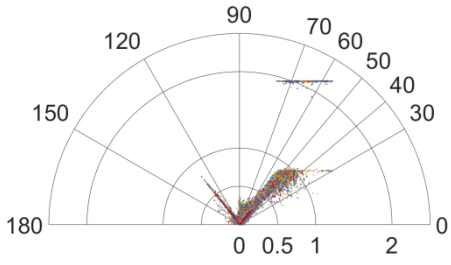

(g_1)

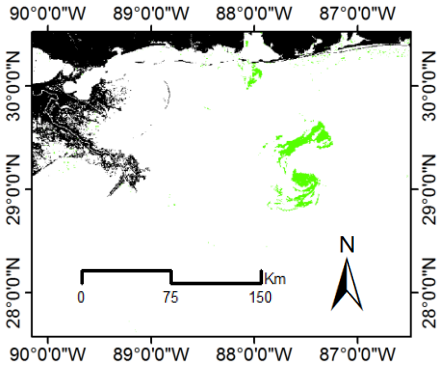

(h)

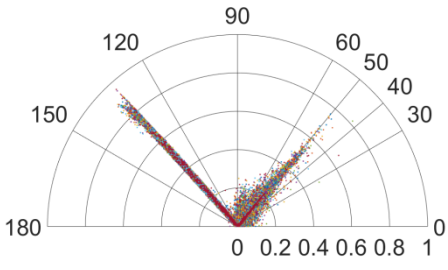

(h_1)

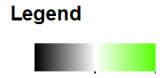

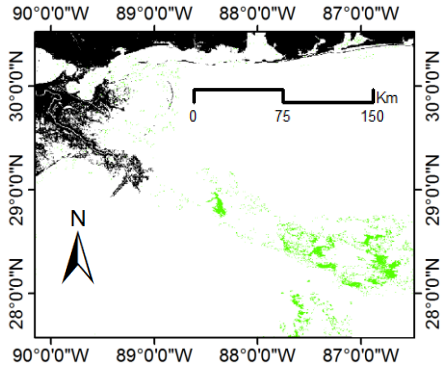

(i)

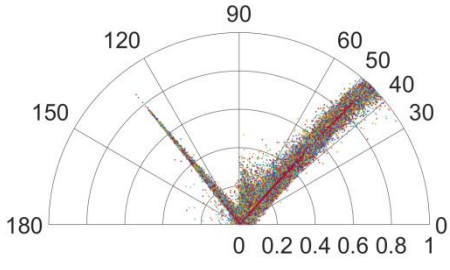

(i_1)

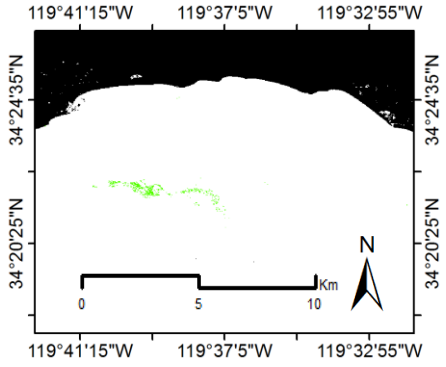

(l)

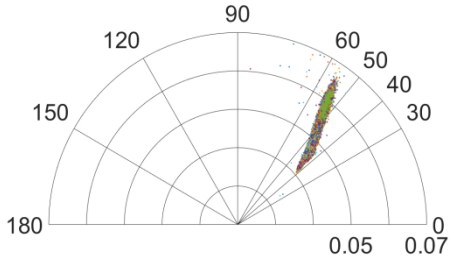

(l_1)

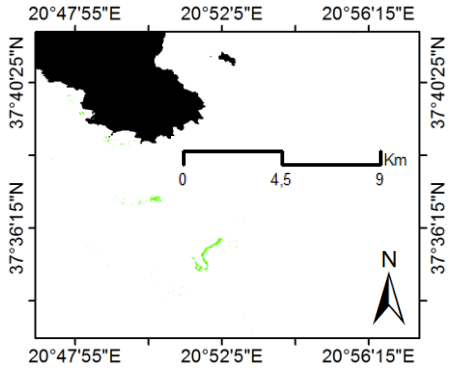

(m)

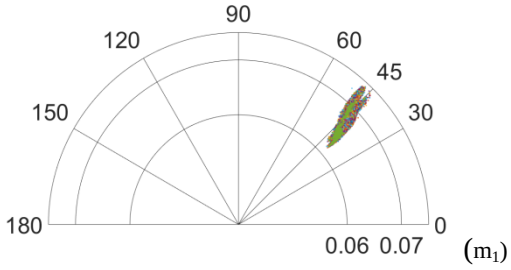

(m_1)

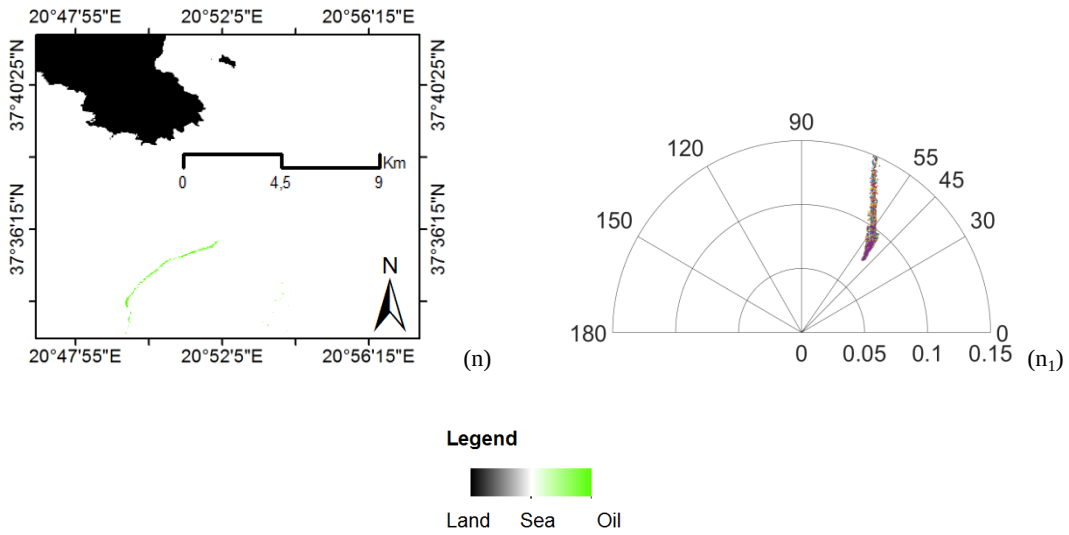

Figure 7. (a) Oil spill detection on April 25, 2010, 18:55 UTC MODIS Aqua; (a1) change vector polar scatter plot related to a; (b) Oil spill detection on April 27, 2010, 17:05 UTC MODIS Terra; (b1) change vector polar scatter plot related to b; (c) Oil spill detection on April 27, 2010, 18:40 UTC MODIS Aqua; (c1) change vector polar scatter plot related to c; (d) Oil spill detection on April 29, 2010, 16:55 UTC MODIS Terra; (d1) change vector polar scatter plot related to d; (e) Oil spill detection on May 9, 2010, 19:05 UTC MODIS Aqua; (e1) change vector polar scatter plot related to e; (f) Oil spill detection on May 17, 2010, 16:40 UTC MODIS Terra; (f1) change vector polar scatter plot related to f; (g) Oil spill detection on May 25, 2010, 19:05 UTC MODIS Aqua; (g1) change vector polar scatter plot related to g; (h) Oil spill detection on May 27, 2010, 18:55 UTC MODIS Aqua; (h1) change vector polar scatter plot related to h; (i) Oil spill detection on July 4, 2010, 16:40 UTC MODIS Terra; (i1) change vector polar scatter plot related to i; (l) Oil spill detection on August 14, 2015, OLI Landsat 8; (l1) change vector polar scatter plot related to l; (m) Oil spill detection on August 6, 2017, OLI Landsat 8; (m1) change vector polar scatter plot related to m; (n) Oil spill detection on August 29, 2017, OLI Landsat 8; (n1) change vector polar scatter plot related to n.

The change vector direction's range is comprised between 40°-50 ° degrees and it does not change due to sun glint contamination.

The OLI data analysis was carried out using bands 1, 2, 4, 5 at 30m spatial resolution in glint free conditions; due to the inability to detect oil spill at sea using bands 4 and 5, we resolve to switch to the more oil sensible bands 1 and 2. The change vector magnitude's threshold is comprised between 0.04-0.1. Thresholds values are now considerable lower due to: (1) the different wavelengths employed during the CVA procedure, (2) the size of the observed oil spills, which is now significantly reduced (from an average extension of 75 km for the Gulf of Mexico oils spills to an average extension of 5 km for both the Refugio Beach and Zakynthos oil spills), and (3) the oil spill quality, which is now characterized by a significant oil in water emulsion. Oil spill features are directionally located within the angular range comprised between 40 ° and 50 ° degrees for both the analysis carried out using respectively MODIS and OLI data. The change vector magnitude is influenced by the quality

and behavior of the oil, as well as by the geometric conditions of observation. The oil spill detection from May 25, 2010 (Figure 7g-g_1) represents a peculiar case. The oil spill is located at the active front of the delta of Mississippi river. Sediment plumes and subsurface plumes had been mixed up with oil in the water column before they reached the shore [45—46].As a result, the section of the spill closest to the shoreline wouldn't have been detected without rising the change magnitude threshold.

Sensor	Band	Wavelength	Resolution	Study area	ED	θ	Result
MODIS							
	Band 1	620-670 nm	500 m	G.M	0.15-0.4	40 °-50 °	Detected
	Band 2	841-876 nm	500 m	G.M	0.15-0.4	40 °-50 °	Detected
OLI							
	Band 4	630-680 nm	30 m	R., Z.	0.15-0.4	40 °-50 °	Not Detected
	Band 5	845-885 nm	30 m	R., Z.	0.15-0.4	40 °-50 °	Not Detected
	Band 1	433-453 nm	30 m	R., Z.	0.04-0.1	40 °-50 °	Detected
	Band 2	450-515 nm	30 m	R., Z.	0.04-0.1	40 °-50 °	Detected

G.M.= Gulf of Mexico; R.=Refugio; Z.=Zakynthos

Table 3. Results Overview

5. Conclusions

A flexible multitemporal and multiplatform semiautomatic procedure for the oil spill detection task was presented in this paper. Oil spill systematic features extraction was carried out on a pixel based by the means of Change Vector Analysis in a multitemporal domain. The proposed methodology has been tested on oil spills of different quality, extension and under different geometric observation conditions. The detection procedure does not rely on sun glint contamination of the scene in order to carry out the oil discrimination.

MODIS sensor provides timely data at medium resolution, allowing to track in detail the Gulf of Mexico oil spill over a three months period. At the same time MODIS imagery proved, as expected, to be ineffective in case of small spills.

On the other hand, OLI Landsat 8 due to the fine resolution, provides much better results than MODIS in detecting small oil spills and natural outflow, although the number of available images is considerably lower.

The results are considered successful and consistent, with a high degree of applicability also to Sentinel 2 data. The proposed methodology is a promising approach towards a fully automatic and multi-platform oil spill detection system. Further method improvement should include: (1) false-positive and look-alike features discrimination improvement; (2) further training and validation through the enrichment of the oil spill datasets; (3) engagement and testing of Sentinel 2 platform in the oil spill detection task.

References

1. Lin I-I, Wen L, Liu K, Tsai W, Liu AK. 2002. Evidence and quantification of the correlation between RADAR backscatter and ocean colour supported by simultaneously acquired in situ sea truth. Geophysical Research Letters, 29(10): 1464, doi:10.1029/2001GL014039.

2. DiGiacomo PM, Washburn L, Holt B, Jones BH. 2004. Coastal pollution hazards in southern California observed by SAR imagery: Stormwater plumes, wastewater plumes, and natural hydrocarbon seeps. Marine Pollution Bulletin, 49: 1013–1024.
3. Brekke C, Solberg AHS. Oil spill detection by satellite remote sensing. Remote Sensing of Environment. 2005; 95: 1–13.
4. Brown CE, Fingas MF. New space-borne sensors for oil spill response. International Oil Spill Conference Proceedings 2001. 2001; 911–916.
5. Fingas M, Brown C. Review of oil spill remote sensing. Marine Pollution Bulletin 2014; 83: 9–23.
6. Werner Alpers, Benjamin Holt, Kan Zeng, Oil spill detection by imaging radars: Challenges and pitfalls, Remote Sensing of Environment 2017; 201: 133-147, ISSN 0034-4257, https://doi.org/10.1016/j.rse.2017.09.002.
7. Otremba Z. (1999). Selected results of light field modeling above the sea surface covered by thin oil film. Computer Simulation and Boundary field problems, Environmental Simulations. 41. pp. 5-13.
8. Otremba Z, Król T. (2001). Light attenuation parameters of polydisperse oil-inwater emulsion. Optica Applicata 31(3): 599–609.
9. Otremba Z, Piskozub J. (2001). Modelling of the optical contrast of an oil film on a sea surface. Optics Express. 9(8): 411–416.
10. Alawadi, Fahad. (2011). Detection and classification of oil spills in MODIS satellite imagery.
11. Long Ma, Ying Li, Yu Liu. 2009. Oil Spill monitoring on its spectral characteristics. Dalian Maritime University, Dalian City, Liaoning Province, China.
12. Lammoglia, Talita, de Souza Filfo, Carlos Roberto. 2010, Spectroscopic characterization of oils yielded from brazilian offshore basins: potential applications of remote sensing. University of Campinas, São Paulo, Brazil.
13. Zhao J, Temimi M, Ghedira H, Hu C. Exploring the potential of optical remote sensing for oilspill detection in shallow coastal waters - A case study in the Arabian Gulf. Optics Express 2014; 22: 13755–13772.
14. Hu C, Li X, Pichel WG, Muller-Karger FE. Detection of natural oil slicks in the NW Gulf of Mexico using MODIS imagery. Geophysical Research Letters 2009, 36, L01604.
15. Hu C, Müller-Karger FE, Taylor C, Myhre D, Murch B, Odriozola AL, Godoy G. MODIS detects oil spills in Lake Maracaibo, Venezuela. Eos Transactions American Geophysical Union 2003; 84: 313–319.
16. Bulgarelli B, Tarchi D. (2006). Exploratory use of MODIS in oil-spill monitoring. In: 2006, Joint Research Centre - Institute for the Protection and Security of the Citizen, pp. 49-60.
17. Bulgarelli B, Djavidnia S. On MODIS retrieval of oil spill spectral properties in the marine environment. IEEE Geoscience and Remote Sensing Letters. 2012; 9: 398–402.
18. Pisano A, Bignami F, Santoleri Rosalia. (2015). Oil Spill Detection in Glint-Contaminated Near-Infrared MODIS Imagery. Remote Sensing. 7. 1112-1134. 10.3390/rs70101112.
19. Olga L, Marina M, Tatiana B, Andrey K, Vladimir K. "Multisensor Approach to

Operational Oil Pollution Monitoring in Coastal Zones," IGARSS 2008 - 2008 IEEE International Geoscience and Remote Sensing Symposium, Boston, MA, 2008, pp. III - 1386-III - 1389.doi: 10.1109/IGARSS.2008.4779619

20. Lee M, Park K, Lee H, Park J, Kang C, Lee M. "Detection and dispersion of oil spills from satellite optical images in a coastal bay," 2016 IEEE International Geoscience and Remote Sensing Symposium (IGARSS), Beijing, 2016, pp. 2491-2494.
21. Qianguo Xing, Lin Li, Mingjing Lou, Lei Bing, Ruxiang Zhao, Zhenbo Li. Observation of Oil Spills through Landsat Thermal Infrared Imagery: A Case of Deepwater Horizon, Aquatic Procedia, 2015; 3: 151-156, ISSN 2214-241X,
22. Liu S, Chi M, Zou Y, Samat A. "A multitemporal change detection solution to oil spill monitoring," 2016 IEEE International Geoscience and Remote Sensing Symposium (IGARSS), Beijing, 2016, pp. 7718-7721. doi: 10.1109/ IGARSS.2016.7731013.
23. Johnson RD, Kasischke ES. (1998) Change vector analysis: A technique for the multispectral monitoring of land cover and condition, International Journal of Remote Sensing 19(3): 411-426, DOI: 10.1080/014311698216062.
24. Ross Lunetta S, Joseph Knight F, Jayantha Ediriwickrema, John Lyon G, Dorsey Worthy L. Land-cover change detection using multi-temporal MODIS NDVI data. Remote Sensing of Environment. 2006; 105(2): 142-154, ISSN 0034-4257.
25. Tobias Landmann, Matthias Schramm, Christian Huettich, Stefan Dech. (2013) MODIS-based change vector analysis for assessing wetland dynamics in Southern Africa. Remote Sensing Letters 4(2): 104-113, DOI: 10.1080/2150704X.2012.699201.
26. Dewi Ratna S, Wietske Bijker, Alfred Stein. Change Vector Analysis to Monitor the Changes in Fuzzy Shorelines. Remote Sensing 2017; 9(2): 147. Doi:10.3390/rs9020147
27. Sicong Liu, Mingmin Chi, angxiu Zou, Alim Samat, Jon Benediktsson, Antonio Plaza. (2017). Oil Spill Detection via Multitemporal Optical Remote Sensing Images: A Change Detection Perspective. IEEE Geoscience and Remote Sensing Letters. PP. 1-5. 10.1109/LGRS.2016.2639540.
28. On scene coordinator report : Deepwater Horizon oil spill. [Washington, D.C. : U.S. Dept. of Homeland Security, U.S. Coast Guard, 2011] xx, 222 p. : col. ill., col. maps ; 28 cm. GC1221 .O52 2011 (https://lccn.loc.gov/2012427375).
29. Kolokoussis P, Karathanassi V. Detection of Oil Spills and Underwater Natural Oil Outflow Using Multispectral Satellite Imagery. International Journal of Remote Sensing Applications 2013; 3: 145–154.
30. Polychronis Kolokoussis, Vassilia Karathanassi. Oil Spill Detection and Mapping Using Sentinel 2 Imagery, Journal of Marine Science and Engineering 2018; 6(1): 4.
31. Srivastava H, Singh T. Assessment and development of algorithms to detection of oil spills using MODIS data. Journal of the Indian Society of Remote Sensing 2010; 38(1): 161–167. Doi:10.1007/s12524-010-0007-9.
32. Ackerman SA, Strabala KI, Menzel WP, Frey RA, Moeller CC, Gumley LE. (1998), Discriminating clear sky from clouds with MODIS. Journal of Geophysical Research. 103(D24), 32141–32157, doi: 10.1029/1998JD200032.
33. Lingjia Gu, Ruizhi Ren, Shuang Zhang. “Automatic Cloud Detection and Removal Algorithm for MODIS Remote Sensing Imagery.” JSW 6 (2011): 1289-1296.

34. Shuguo Chen, Tinglu Zhang. (2015). An improved cloud masking algorithm for MODIS ocean colour data processing. Remote Sensing Letters. 6, 218-227. 10.1080/2150704X.2015. 1026955.
35. Department of the Interior U.S. Geological Survey Product guide: Landsat 8 surface reflectance code (LASRC) product. USGS, Version 4.3, March 2018, https://landsat.usgs.gov/sites/ default/files/documents/lasrc_product _guide.pdf
36. Cox C, Munk W. Statistics of the Sea Surface Derived from Sun Glitter. The Journal of Marine Research 1954; 13: 198-227.
37. McFEETERS SK (1996) The use of the Normalized Difference Water Index (NDWI) in the delineation of open water features. International Journal of Remote Sensing 17(7): 1425-1432, DOI: 10.1080/01431169608948714.
38. Jensen J. (1996). Introductory digital image processing. A remote sensing perspective. 2nd Edition. New Jersey: Prentice Hall.
39. Lambin EA, Strahler AH. (1994). Indicators of land cover change for change vector analysis in multitemporal space at coarse spatial scales. International Journal of Remote Sensing 15: 2099–2119.
40. Fingas M, Brown CE. Oil Spill Remote Sensing: A Review, Chapter 6, in Oil Spill Sci. Techn., M. Fingas, Editor, Gulf Publishing Company, NY, NY, 111, 2011.
41. Taravat A, Del Frate. Development of band ratioing algorithms and neural networks to detection of oil spills using Landsat ETM+ data. F. EURASIP Journal on Advances in Signal Processing. (2012) 2012: 107. https://doi.org/10.1186/1687-6180-2012-107.
42. Clark RN, Leifer I, Livo KE, Kokaly R, Hoefen TM, Bradley ES, *et al.* & AVIRIS Team, 2010, A method for quantitative mapping of Oil Spills using imaging spectroscopy. US Geological Survey, Reston, Virginia, USA.
43. Skytruth imagery, Deepwater Horizon Blowout, April 2010 - https://www.skytruth.org /tech/skytruthimagery/flickrcontent/5417802 -72157619746190793/72157623909364472.
44. Skytruth imagery Oil Closes Another California Beach, August 2015-https://www. skytruth.org /2015/08/oil-closes-another-california-beach.
45. Yan B, Passow U, Chanton JP, Nöthig E-M, Asper V, Sweet J, Pak D. (2016). Sustained deposition of contaminants from the Deepwater Horizon spill. Proceedings of the National Academy of Sciences of the United States of America, 113(24), E3332–E3340. http://doi.org/10.1073/pnas.1513156113.
46. Ryerson TB, Camilli R, Kessler JD, Kujawinski EB, Reddy CM, Valentine DL, Atlas E, Blake DR, de Gouw J, Meinardi S, Parrish DD, Peischl J, Seewald JS, Warneke C. Chemical data quantify Deepwater Horizon hydrocarbon flow rate and environmental distribution, Proceedings of the National Academy of Sciences of the United States of America. 109 (2012), pp. 20246-20253, 10.1073/pnas.1110564109.